Journal of Structural Biology: X 10 (2024) 100112

Contents lists available at ScienceDirect

Journal of Structural Biology: X

journal homepage: www.sciencedirect.com/journal/journal-of-structural-biology-x

Research Article

Structural analysis of the stable form of fibroblast growth factor 2 – FGF2-STAB

Gabin de La Bourdonnaye [a,b], Martin Marek [a,c], Tereza Ghazalova [b], Jiri Damborsky [a,c], Petr Pachl [d], Jiri Brynda [d], Veronika Stepankova [b], Radka Chaloupkova [a,b,*]

[a] Loschmidt Laboratories, Department of Experimental Biology and RECETOX, Faculty of Science, Masaryk University, Brno, Czech Republic
[b] Enantis Ltd., Biotechnology Incubator INBIT, Brno, Czech Republic
[c] International Clinical Research Center, St. Anne's University Hospital, Brno, Czech Republic
[d] Institute of Organic Chemistry and Biochemistry, Academy of Sciences of the Czech Republic, Prague, Czech Republic

ARTICLE INFO

Keywords:
Stabilized fibroblast growth factor 2
X-ray structural analysis
Protein flexibility

ABSTRACT

Fibroblast growth factor 2 (FGF2) is a signaling protein that plays a significant role in tissue development and repair. FGF2 binds to fibroblast growth factor receptors (FGFRs) alongside its co-factor heparin, which protects FGF2 from degradation. The binding between FGF2 and FGFRs induces intracellular signaling pathways such as RAS-MAPK, PI3K-AKT, and STAT. FGF2 has strong potential for application in cell culturing, wound healing, and cosmetics but the potential is severely limited by its low protein stability. The thermostable variant FGF2-STAB was constructed by computer-assisted protein engineering to overcome the natural limitation of FGF2. Previously reported characterization of FGF2-STAB revealed an enhanced ability to induce MAP/ERK signaling while having a lower dependence on heparin when compared with FGF2-wt. Here we report the crystal structure of FGF2-STAB solved at 1.3 Å resolution. Protein stabilization is achieved by newly formed hydrophobic interactions, polar contacts, and one additional hydrogen bond. The overall structure of FGF2-STAB is similar to FGF2-wt and does not reveal information on the experimentally observed lower dependence on heparin. A noticeable difference in flexibility in the receptor binding region can explain the differences in signaling between FGF2-STAB and its wild-type counterpart. Our structural analysis provided molecular insights into the stabilization and unique biological properties of FGF2-STAB.

Introduction

The fibroblast growth factor (FGF) family is a group of secreted signaling proteins that play multiple roles in tissue development and repair (Ornitz and Itoh, 2015). FGF2, also referred to as basic fibroblast growth factor, bFGF, or heparin-binding growth factor 2, belongs to one of five paracrine-acting subfamilies of FGFs that interact with heparin as a co-factor to bind FGF receptors (FGFRs). FGF2 preferentially interacts with FGFR1c and FGFR3c receptors but exhibits some activity also towards FGFR1b and FGFR2c (Hui et al., 2018; Ornitz and Itoh, 2015). The specific interaction of FGF2 with FGFR triggers receptor dimerization and autophosphorylation of its tyrosine kinase domain which leads to the activation of intracellular signaling pathways such as RAS-MAPK (ERK1/2), PI3K-AKT, PLCγ −PKC, and STAT (Nugent and Iozzo, 2000; Ornitz and Itoh, 2015).

The assumed role of heparin (heparan sulfate proteoglycans) in FGF2 signaling is stabilization of the ternary complex containing FGF2, heparin, and FGFR. As a part of the complex, heparin increases the affinity of FGF2 to FGFR and decreases the rate of dissociation of FGF2 from FGFR (Belov and Mohammadi, 2013; Ibrahimi et al., 2004; La Venuta et al., 2015; Ornitz and Itoh, 2015). Heparin also protects FGF2 molecules on cell surfaces against thermal and proteolytic degradation and thus prolongs FGF2 biological action (Caldwell et al., 2004; La Venuta et al., 2015; Paluck et al., 2016). During the FGF2 lifetime, heparin further mediates the final step of FGF2 secretion via supporting FGF2 diffusion through the cellular membrane barrier leading to increased efficiency of FGF2 translocation into the cells (La Venuta et al., 2015; Zehe et al., 2006). Although heparin is expected to mediate FGF2 signaling, several studies reported that FGF2 can interact with FGFRs without the intervention of heparin/heparan sulfate and trigger the activation of signaling pathways (Fannon and Nugent, 1996; Nugent and Edelman, 1992). However, long-term activation of the signaling

* Corresponding author.
E-mail address: chaloupkova@enantis.com (R. Chaloupkova).

https://doi.org/10.1016/j.yjsbx.2024.100112
Received 4 July 2024; Received in revised form 24 September 2024; Accepted 14 October 2024

pathway, and long-lasting biological response has been shown to require the presence of heparin (Zhu et al., 2010; Delehedde et al., 2002).

Through the activation of downstream signaling pathways, FGF2 plays an important role in regulating proliferation, differentiation, migration, and survival of a wide variety of cell types (Bikfalvi et al., 1997; Javerzat et al., 2002). FGF2 is used in fields such as pluripotent stem cell cultivation (Amit et al., 2000; Levenstein et al., 2006; Xu et al., 2005) and therapeutic tissue regeneration (Barrientos et al., 2014; Hui et al., 2018; Yun et al., 2010). Like most members of the FGF family, the application potential of FGF2 is limited by its intrinsic instability. In therapeutics (Buchtova et al., 2015; Chen et al., 2012), daily administration of FGF2 is needed due to its short half-life *in vivo* ($\leq$ 10 h at 37 °C), which may be time-consuming and painful for patients and may cause potential risk of infection. Even in the case of stem cell cultures, the instability of FGF2 leads to impractical, expensive protocols and inefficient workloads in which fresh FGF2 must be regularly supplemented to the cultivation media (Lotz et al., 2013).

FGF2-STAB, a highly thermostable variant of FGF2 stabilized by a computer-assisted protein engineering approach, has been reported by Dvorak et al. (Dvorak et al., 2018, 2017). FGF2-STAB is a nine-point mutant of human FGF2 that exhibits an enhanced melting temperature of up to 19 °C and a prolonged functional half-life *in vitro* at 37 °C from 10 h up to more than 20 days. Moreover, it is fully able to engage FGFR downstream signaling pathways, to maintain the undifferentiated state of human embryonic stem cells, and to inhibit the chondrocyte growth. In fact, FGF2-STAB showed improved biological activity when compared with the wild-type (Dvorak et al., 2018). Koledova et al. also demonstrated that FGF2-STAB is less dependent on heparin for activation of ERK signaling compared to the wild-type (Koledova et al., 2019). FGF2-STAB thus represents an attractive alternative to FGF2-wt for therapeutic and stem cell cultivation applications. In this article, we describe the crystallization and structural analysis of FGF2-STAB to get structural insight into its unique properties.

Material and methods

Protein expression and purification

The gene encoding FGF2-STAB was commercially synthesized (GeneArt, Life Technologies) and subcloned into the pET28b-His-thrombin expression vector between NdeI and XhoI restriction sites (Table 1).

The *fgf2-STAB* gene containing the 9 stabilizing mutations (see Supplementary Table S1) was expressed in *Escherichia coli* under control of the T7lac promoter and the gene expression was induced by the addition of isopropyl β-D-thiogalactopyranoside (IPTG). Chemically competent *E. coli* BL21(DE3) cells were transformed with the recombinant expression vector pET28b-His-thrombin::*fgf2-STAB* using the heat shock method. The transformed cells were plated on LB agar plates supplemented with Kanamycin (50 μg/ml) and incubated overnight at 37 °C. Single colonies were used for inoculation of 10 ml of LB medium (Sigma–Aldrich, USA) supplemented with Kanamycin (50 μg/ml). The culture was grown overnight at 37 °C and used to inoculate 1000 ml of LB medium supplemented with Kanamycin (50 μg/ml). The cells were grown at 37 °C and 115 RPM. When the culture reached an optical density of 0.6 at 600 nm, the induction of protein expression (at 20 °C) was initiated by the addition of IPTG to a final concentration of 0.5 mM, and the cells were cultivated overnight. The cells were harvested, washed, and resuspended in equilibrating buffer (20 mM potassium phosphate buffer, pH 7.5; 0.5 M NaCl, 10 mM imidazole) and stored at −80 °C. The cell suspension was disrupted by sonication using a UP200S ultrasonic processor (Hielscher, Germany) and centrifuged for 1 h at 4 °C at 21,000 g. The cell-free extract (supernatant) was collected and purified on a cOmplete His-Tag Purification Column (Merck, Germany) attached to an ÄKTA FPLC purification system (GE Healthcare, USA). His-tagged protein was bound to the resin in equilibrating buffer. Unbound and weakly bound proteins were washed out. His-tagged protein was eluted by a linear gradient (0 – 100 %) of purification buffer containing 500 mM imidazole. The eluted protein was pooled and dialyzed overnight against 50 mM Tris-HCl buffer, pH 7.5, containing 250 mM sodium chloride. Bradford reagent (Merck, USA) was used to determine the protein concentration, with bovine serum albumin (Merck, Germany) used as a standard.

Table 1
Production specifics of FGF2-STAB.

DNA source	Synthesized DNA
Number of amino acids	175 (including His-tag)
Molecular weight of the protein	19497.20 Da (including His-tag)
Commercially subcloned into	pET28b (NdeI/XhoI), Kan^R
Expression host	*E. Coli* BL21(DE3)
Complete amino acid sequence[a] of the construct	MGSSHHHHHHSSGLVPRGSH**M**AAGSI TTLPALPEDGGSGAFPPGHFKDPKLL YCKNGGFFLRIHPDGRVDGTRDKSDP FIKLQLQAEERGVVSIKGVCANRYLA MKEDGRLYAIKNVTDECFFFERLEEN NYNTYRSRKYPSWYVALKRTGQYKLG SKTGPGQKAILFLPMSAKS

[a] The amino acid sequence of FGF2-STAB with upstream sequence in pET28b vector. The sequence of N-terminal 6x His-tag and thrombin cleavage site is underlined, N-terminal methionine is in bold. The amino acid numbering used herein corresponds to the sequence of human FGF2-wt (UniProt entry P09038-2), i.e. starts from N-terminal methionine.

Protein crystallization

The crystallization experiments were conducted with freshly purified FGF2-STAB concentrated to 6–8 mg/ml and stored at 4 °C maximally for 24 h. The purity of the protein was checked by 10 % sodium dodecyl sulfate–polyacrylamide gel electrophoresis (SDS-PAGE) followed by Coomassie Brilliant Blue staining. Various commercial screens were employed for screening of FGF2-STAB initial crystallization conditions including Index (Hampton Research, USA), JSCG, Mem Gold, Mem Gold 2, Midas, Morpheus, Pact Premier, PGA Eco, SG, and Wizard screens (Molecular Dimensions, United Kingdom). The crystallization screening was performed in 96-well MRC 2 Lens Crystallization Plates (SWISSCI, United Kingdom) using the sitting-drop vapor-diffusion method. 0.1–0.2 μl of protein solution was mixed with the reservoir solution in the ratios 1:1 and 2:1 using the crystallization robot Gryphon LCP (Art Robbins Instruments, USA) and equilibrated against 50 μl of the reservoir solution. Successful crystallization conditions identified by the initial screening were optimized by varying pH conditions, salt, protein, and precipitant concentrations, and upscaling the drop volume on EasyXTal 15-well plates (Qiagen, Germany) using the vapor-diffusion hanging-drop method. For the scale-up experiments, 1 or 2 μl of protein solution was mixed with the reservoir solution in the protein to precipitant ratios 1:1 and 2:1 and equilibrated against 500 μl of a reservoir solution. The plates were incubated at 19 °C.

Data collection

The selected FGF2-STAB crystals were cryoprotected by the addition of 20% 2-methyl-2,4-pentanediol and 15% D-maltose into the drop and subsequently mounted on nylon cryoloops (Hampton Research, USA) immediately followed by flash-cooling in liquid nitrogen. X-ray diffraction patterns of successfully optimized crystals were measured on a laboratory X-ray diffractometer HF007 (Rigaku, Japan) operated at IOCB, Prague. The conditions resulting in crystals diffracting at the highest resolution were selected for complete diffraction data collection. Complete diffraction data were collected on the MX14.1 beamline (Mueller et al., 2015) operated by the Helmholtz-Zentrum Berlin (HZB) at the BESSY II electron-storage ring, Berlin-Adlershof, Germany. Diffraction data collection statistics are summarized in Table 2.

Table 2
Diffraction data collection and refinement statistics.

	FGF2-STAB
X-ray diffraction data collection statistics	
X-ray source	BESSY II – BL14.1
Space group	*C*121
Cell parameters	
a, *b*, *c* (Å)	117.51, 38.67, 34.26
α, *β*, *γ* (°)	90.00, 104.64, 90.00
Number of molecules in AU	1
Wavelength (Å)	0.9184
Resolution range (Å)	33.15 - 1.31 (1.36 - 1.31)
Observed reflections	101,176
Number of unique reflections	35,777 (3,496)
Completeness (%)	99.37 (97.84)
Multiplicity	3.38
I/σ (I)	15.28 (1.17)
R_{merge} [a]	0.6 (1.8)
$CC_{1/2}$ [b]	0.999 (0.512)
Refinement statistics	
Resolution (Å)	1.3
No. of reflections in working set	35,765 (3,487)
R_{work} [c] / R_{free} [d]	0.197 (0.365) / 0.227 (0.376)
RMSD bond length (Å)	0.005
RMSD angle (°)	0.800
Ramachandran favored (%)	99
Ramachandran allowed (%)	1
Ramachandran outliers (%)	0
Contents of asymmetric unit	
No. of atoms in AU	1,270
No. of protein atoms in AU	1,151
No. of protein residues	134
No. of water molecules in AU	126
Mean B values	
Protein (Å^2)	26.59
Waters (Å^2)	36.35
PDB code	8OM6

Values in parentheses are for the highest resolution shell.

[a] $R_{merge} = \Sigma_{hkl}\Sigma_i |I_i(hkl) - \langle I(hkl)\rangle| / \Sigma_{hkl}\Sigma_i I_i(hkl)$, where the $I_i(hkl)$ is the *i*th observation of reflection *hkl* and $\langle I(hkl)\rangle$ is the weighted average intensity for all observations of reflection *hkl*.

[b] As described by Karplus and Diederichs (Karplus and Diederichs, 2012).

[c] R_{work} value = $||F_o| - |F_c||/|F_o|$, where F_o and F_c are the observed and calculated structure factors, respectively.

[d] R_{free} is equivalent to R_{work} value, but is calculated for 5% of the reflections chosen at random and omitted from the refinement process.

Structure determination and refinement

The structure of FGF2-STAB was solved by molecular replacement using MOLREP software (Vagin and Teplyakov, 2010) implemented in the CCP4 package (Winn et al., 2011) and the structure of wild-type human fibroblast growth factor 2 (PDB ID 4FGF (Eriksson et al., 1993)) as a search model from which ions, ligands, and water molecules had been removed. Automatic structural refinement of FGF2-STAB was carried out using REFMAC v5.8 (Murshudov et al., 2011) and Phenix. refine from the Phenix software package (Adams et al., 2010) always using the anisotropic B-factor model. The Coot software was used to manually refine the data using $2F_o$-$2F_c$ and F_o-F_c electron density difference maps between each step of automatic refinement (Emsley et al., 2010). The quality of the final structural model was validated using tools provided in Coot (Emsley et al., 2010) and MolProbity (Chen et al., 2010). The refinement statistics are summarized in Table 2. Figures showing structural representations were made using PyMOL v1.5.04 (Schrödinger, LLC). Atomic coordinates and experimental structure factors have been deposited in the Protein Data Bank under PDB code 8OM6. The amino acid numbering used in the FGF2-STAB structure corresponds to the sequence of human FGF2-wt (UniProt entry P09038-2), i.e., it starts from N-terminal methionine. Negative numbering is therefore used for N-terminal 6x His-tag and thrombin cleavage site.

In silico analysis of protein dynamics

Parallelly with the crystallographic analysis, molecular dynamics (MD) simulations were used to analyze the flexibility of FGF2-STAB (structure solved in this study, PDB ID 8OM6) and FGF2-wt (PDB ID 4FGF (Eriksson et al., 1993)) in order to eliminate overinterpretation of restricted mobility of the side chains caused by close interactions of neighboring molecules due to crystal-packing constraints. All water and ligand molecules were removed from the structures. Then, the H++ web server (Anandakrishnan et al., 2012) was used to add the missing hydrogens, adjust the pH to 6.5, and create a water box with an edge distance of 10 Å using the TIP3P water model. The systems were first minimized using the conjugate-gradient method for 500 steps followed by 500 conjugate-gradient steps with a decreasing restraint on the protein backbone (500, 125, 50, 25, and 5 kcal mol^{-1} Å^{-2}). The simulations employed periodic boundary conditions using the particle mesh Ewald method (Harvey and De Fabritiis, 2009) for the treatment of interactions beyond a 10 Å cut-off, electrostatic interactions were suppressed > 4 bond terms away from each other, and all bonds containing hydrogens were fixed by SHAKE algorithm (Elber et al., 2011) with 2 fs time steps. The equilibration simulation consisted of two steps: (i) 20 ps of gradual heating from 0 to 310 K under constant volume using a Langevin thermostat with a collision frequency of 1.0 ps^{-1}, and with harmonic restraints of 5.0 kcal mol^{-1} Å^{-2} on the position of all protein atoms, and (ii) 2000 ps of unrestrained MD at 310 K using the Langevin thermostat, and the constant pressure of 1.0 bar using pressure coupling constant of 1.0 ps^{-1} employing the Berendsen thermostat. The 300 ns production runs were started with the files resulting from the equilibration and the same settings as the last step of the equilibration MD. The trajectories were saved every 100 ps. All calculations were carried out in the GPU (CUDA) PMEMD module (Götz et al., 2012; Salomon-Ferrer et al., 2013) of AMBER 16 (Case et al., 2023) using ff14 force field (Cerutti et al., 2014) in three independent replications.

Results and discussion

FGF2-STAB crystallization and X-ray data collection

A freshly isolated and purified sample of FGF2-STAB concentrated to 6–8 mg/ml in a 50 mM Tris-HCl buffer with 250 mM sodium chloride was used for the initial screening of suitable crystallization conditions. The initial screening led to the formation of small three-dimensional crystals of FGF2-STAB. The crystals appeared after 4–6 weeks of incubation at 19 °C in the drop composed of the protein mixed with the precipitant solution consisting of 0.1 M Bis-Tris buffer, pH 6.5, and 25 % (w/v) PEG 3350 in a 1:1 ratio.

The identified condition was further optimized to prepare single crystals of FGF2-STAB with sufficient size and quality for diffraction data collection. Variation of pH, protein and precipitant concentration, and protein to precipitant ratio resulted in the growth of tetragonal crystals of FGF2-STAB (Supplementary Figure S1), which appeared after 10–11 weeks of incubation at 19 °C in the drop prepared by mixing of FGF2-STAB in a concentration of 3.4 mg/ml with the crystallization solution consisting of 0.1 M Bis-Tris buffer, pH 6.3, and 19 (w/v %) PEG 3350 in a ratio 2:1. These crystals were used for X-ray diffraction data collection and a complete data set was collected to 1.3 Å resolution. The data collection statistics are presented in Table 2. The crystals belonged to the primitive monoclinic space group *C*121 with unit-cell parameters a = 117.51, b = 38.67, c = 34.26 Å, α = γ = 90°, β = 104.64°. The calculated Matthews coefficient (V_M) of 1.93 Å^3 Da^{-1} implies that the crystal contains one molecule per asymmetric unit with an estimated solvent content of 36.32 %.

Structural analysis of FGF2-STAB

The structural model of FGF2-STAB was obtained by molecular

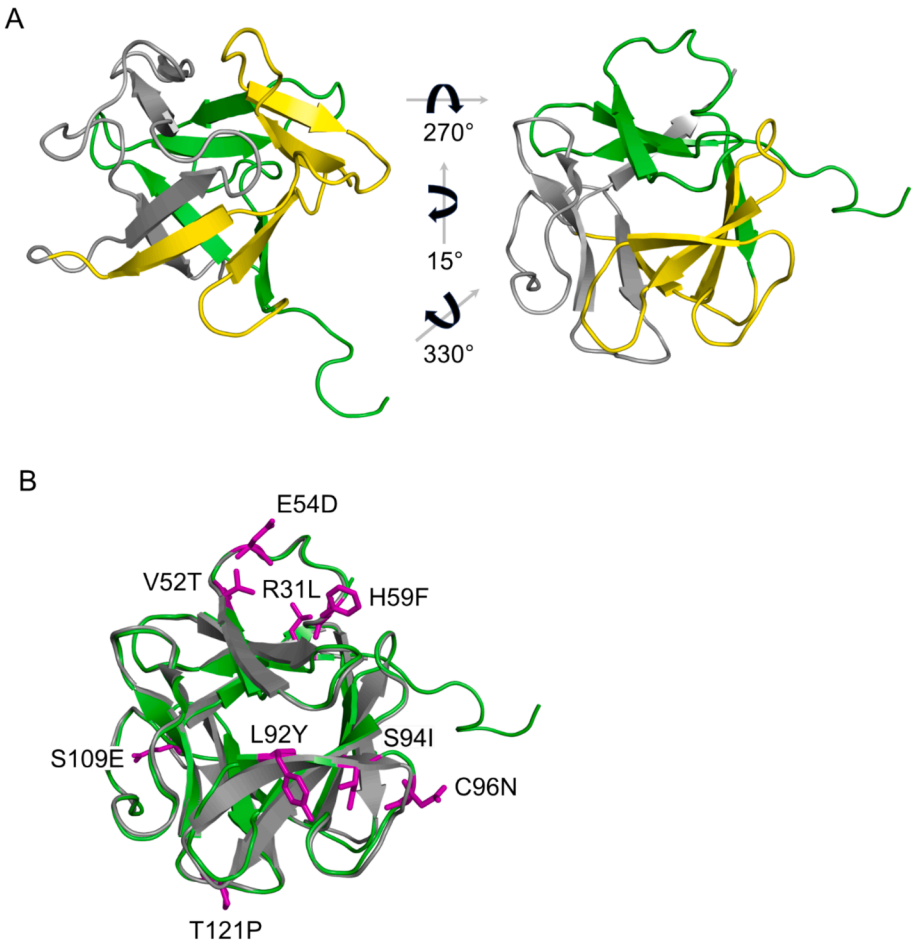

Fig. 1. X-ray structural analysis of FGF2-STAB. (A) The overall structure of FGF2-STAB exhibits a β-trefoil fold. The three β-trefoil units, each formed by two β-hairpins, are depicted in green, grey, and yellow color. One β-hairpin of each unit forms part of a six-stranded β-barrel (left, lower part), and the other forms part of the triangular β-hairpin triplet (left, upper part). (B) Superimposition of the crystal structures of FGF2-STAB (PDB ID 8OM6) and FGF2-wt (PDB ID 4FGF (Eriksson et al., 1993)) shown in green and grey, respectively. The introduced stabilizing mutations in FGF2-STAB are shown as magenta sticks. (For interpretation of the references to color in this figure legend, the reader is referred to the web version of this article.)

replacement using the structure of FGF2-wt (PDB ID 4FGF (Eriksson et al., 1993)) as a search model. The final structural model of FGF2-STAB, validated using tools provided in Coot (Emsley et al., 2010) and MolProbity (Chen et al., 2010) contains the amino acid residues 21–154. All residues are within allowed Ramachandran regions with 99 % of residues in the most favored Ramachandran regions (Table 2). The overall structure of FGF2-STAB is composed of 12 antiparallel β-strands, forming six β-hairpins. Three of the hairpins form a six-stranded β-barrel structure capped by a triangular β-hairpin triplet (Fig. 1A). The overall fold of FGF2-STAB referred to as the β-trefoil (Murzin et al., 1992) is formed by three similar units of super-secondary structure, each of which consists of two β-hairpins (4 β-strands) arranged in "Y" or trefoil shape. The three units are associated so that one β-hairpin of each unit forms part of the β-barrel structure, and the other forms part of the triangular β-hairpin triplet (Fig. 1A) giving the FGF2-STAB structure a shape of trigonal pyramid. Comparison of the FGF2-STAB structure with the FGF2-wt (PDB ID 4FGF (Eriksson et al., 1993)) revealed that the protein backbones had highly similar geometry, with a calculated RMSD value of 0.31 Å for the overlaps of Cα atoms (Fig. 2). This observation is consistent with the previously performed analysis of the secondary structure of FGF2-STAB by CD spectroscopy (Dvorak et al., 2018), which did not reveal any conformational changes after introducing the stabilizing mutations.

FGF2-STAB differs from FGF2-wt in the surface region responsible for interaction with FGFR

A clear difference between the two compared structures lies in the spatial arrangement of the surface region formed by amino acids 102–117 arranged in a β-chain-β-turn-β-chain structural motif (Fig. 2). This amino acid region is responsible for the interaction of the FGF2 protein with the FGF receptor, through amino acids E105, E108, S109, N110, N111, Y112, N113, and Y115 (Plotnikov et al., 2000, 1999). One of these amino acids, Ser109, was replaced by Glu in the FGF2-STAB structure. Structural alignment of FGF2-STAB with available FGF2-wt crystal structures with a resolution below 2 Å revealed that this structural region, together with the N-terminal part of the protein, is one of FGF2's most flexible regions (Fig. 2). Since the introduced stabilizing mutations did not cause a decrease in the biological activity of the protein (Dvorak et al., 2018; Koledova et al., 2019) it can be speculated that the identified difference between the structure of FGF2-STAB and FGF2-wt is due to the natural flexibility of this surface region rather than the introduced mutation. On the other hand, the S109E substitution could be responsible for the increased efficiency of FGF2-STAB in FGFR-mediated cell response previously reported by Koledova et al. (Koledova et al., 2019), since the other amino acids participating in the interaction with FGF receptors were not mutated and stayed structurally conserved.

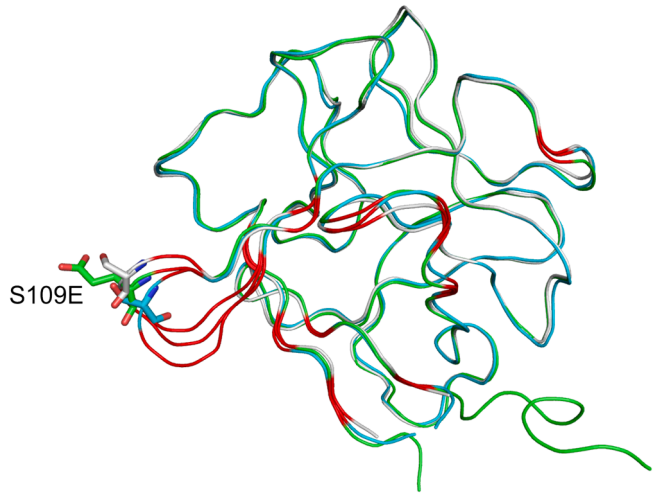

Fig. 2. Superimposition of crystal structures of FGF2-STAB (PDB ID 8OM6) and FGF2-wt (PDB IDs 4FGF (Eriksson et al., 1993) and 2FGF (Zhang et al., 1991)) with highlighted amino acids residues involved in FGFR binding interaction (see Supplementary Figure S2). The Cα backbone atoms of FGF2-STAB and FGF2-wt are shown as green, cyan (PDB ID 4FGF (Eriksson et al., 1993)), and grey (PDB ID 2FGF (Zhang et al., 1991)) ribbon, respectively. The most distinct part between the compared structures, formed by amino acid residues 102–117, is highlighted in red. This highly flexible surface region is involved in FGFR binding interaction. Other amino acid sites involved in FGFR interaction are also highlighted in red. The S109E substitution/S109 residue located in the flexible surface region is shown by a stick model, where the color of the C atoms corresponds to the color of the ribbon model of the respective protein. (For interpretation of the references to color in this figure legend, the reader is referred to the web version of this article.)

Modified dynamics of FGF2-STAB could explain its higher efficiency in ERK signaling

Although the amino acids responsible for the interaction of the protein with heparin were not affected by mutagenesis, FGF2-STAB demonstrated significantly lower dependence on heparin to induce ERK signaling (Koledova et al., 2019). The decreased heparin dependence was linked with a reduced binding affinity (6.2-fold higher K_d) of FGF2-STAB for heparin (Koledova et al., 2019). As previously demonstrated on closely related FGF1 protein and its stable variants (Zakrzewska et al., 2005), the main role of heparin in FGFR-mediated cell signaling is protein stabilization, and heparin is not essential for FGF1-FGFR interaction and FGFR activation. The lower stabilization effect of heparin on FGF2-STAB when compared with FGF2-wt, demonstrated by the lower difference in melting temperature of the protein with and without heparin, was simultaneously observed (Koledova et al., 2019). To investigate whether the lower FGF2-STAB dependence on heparin could relate to decreased protein flexibility caused by its stabilization, we compared B-factors of FGF2-STAB and FGF2-wt structures after 3 runs of 300 ns-long MD simulations. The MD simulations were performed in order to eliminate overinterpretation of restricted mobility of the protein side chains caused by crystal-packing constraints. B-factors obtained from MD simulations better approximate the intrinsic flexibility of the protein in the solution, compared to the crystallographic B-factors, since MD analyses are performed in the explicit solvent (Caldararu et al., 2019). The analysis revealed that most amino acids in both investigated protein structures exhibited similar B-factor values (Fig. 3). No difference in flexibility of the amino acid regions involved in heparin interaction was identified. The only difference in flexibility between FGF2-STAB and FGF2-wt was identified in the amino acid region formed by amino acid residues 105–112 (Fig. 3). This amino acid region represents the part of the structure with the highest flexibility in both proteins and, at the same time, the part of the FGF2 structure responsible for the interaction with FGF receptor (Plotnikov et al., 2000, 1999). Interestingly, the amino acid region formed by residues 105–112 in FGF2-STAB exhibited higher flexibility than the corresponding region in FGF2-wt (Fig. 3, Supplementary Table S2). The highest B-factor was identified at position 109, which was mutated in FGF2-STAB. This locally induced flexibility of the surface region upon introducing the mutation could be a possible explanation for the previously observed increased efficiency of FGF2-STAB to promote FGFR-mediated cell response (Dvorak et al., 2018; Koledova et al., 2019).

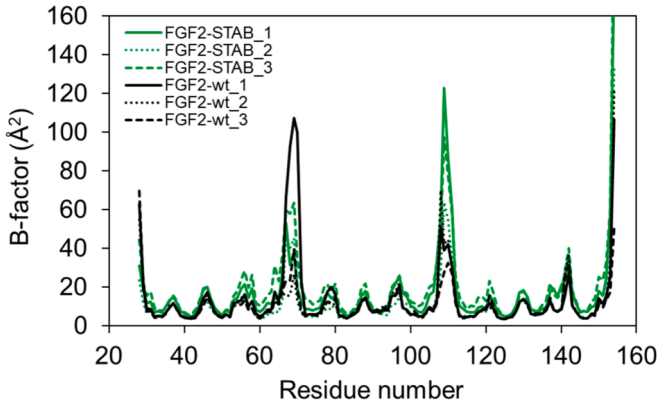

Fig. 3. Comparison of B-factor values from three runs of 300-ns long MD simulations for FGF2-STAB and FGF2-wt.

The follow-up analysis of the secondary structure elements' evolution in the most flexible region of FGF2-STAB and FGF2-wt structures revealed another difference between the two proteins. While the formation of the 3_{10}-helix occasionally transitioning into an antiparallel β-strand or β-turn was observed for the amino acids 109–112 in FGF2-wt, the corresponding region in FGF2-STAB consistently formed a β-turn throughout the whole simulation (Supplementary Figure S3). The formation of the 3_{10}-helix, a secondary element stabilized by a hydrogen bond between the carbonyl oxygen of the i^{th} amino acid and the amide hydrogen of the i^{th+3} amino acid, could be a possible explanation for lower flexibility of the region formed by amino acids 109–112 in FGF2-wt. The previously solved crystal structure of FGF2-wt complexed with immunoglobulin-like domains 2 and 3 of FGFR1 receptor revealed that the amino acid region formed by Ser109, Asn110, and Asn111 undergoes conformational shift to optimize the interaction with the receptor (Plotnikov et al., 1999). We hypothesized that higher flexibility of the β-turn formed by Glu109, Asn110, and Asn111 in FGF2-STAB allows easier structural rearrangement upon the interaction with the receptor, resulting in the higher efficiency of ERK signaling activation when compared with FGF2-wt.

Investigation of intramolecular hydrogen bonds stabilizing the backbone atoms in the flexible region formed by amino acid residues 109–112 revealed the possible formation of three hydrogen bonds in FGF2-wt versus one hydrogen bond in FGF2-STAB over the whole MD simulations. In FGF2-wt, the carbonyl oxygen of Tyr112 can form a hydrogen bond with the amide hydrogen of Ser109, the carbonyl oxygen of Ser109 can form a hydrogen bond with the amide hydrogen of Asn111, and the carbonyl oxygen of Ser109 can form a hydrogen bond with the amide hydrogen of Tyr112. On the contrary, only the formation of a hydrogen bond between the carbonyl oxygen of Glu109 and the amide hydrogen of Asn111 was identified in MD simulations for FGF2-STAB. The introduction of S109E substitution to FGF2-STAB disabled the formation of hydrogen bonds between the backbone atoms of Ser109 and Tyr112 likely responsible for the stabilization of the 3_{10}-helix observed in MD simulations for FGF2-wt. This observation corroborates the higher flexibility of the surface region formed by amino acids 109–112 in FGF2-STAB.

Analysis of the B-factors further revealed another flexible region in both FGF2 proteins formed by amino acid residues 65–71. Interestingly,

this region, particularly the amino acids 65–69, also contributes to FGF2 interaction with FGFR, as previously reported by Plotnikov et al. (Plotnikov et al., 1999). Although no statistically important difference in flexibility of this region between the FGF2-wt and FGF2-STAB was identified (Supplementary Table S2), it seems that local flexibility of surface amino acid regions is important for proper binding interaction of FGF2 protein with the receptor.

Structural basis of enhanced stability of FGF2-STAB

The effect of individual substitutions on FGF2-STAB structure was further investigated to get structural insight into FGF2 stabilization. Identified modifications in FGF2-STAB structure caused by particular substitution were correlated with previously reported stabilizing effects of the mutation (Supplementary Table S1, (Dvorak et al., 2018)). Significant enhancement of intramolecular hydrophobic interactions was observed in the case of R31L and H59F substitutions. Replacement of Arg31 by Leu promoted the formation of new hydrophobic interactions with the side chains of the spatially neighboring amino acids Phe60, Lys75, Ile80, Met171, and Ala173 (Fig. 4A). This observation nicely correlates with the fact that R31L is the substitution with the highest contribution to protein stabilization (ΔT_m = 4 °C) out of the nine introduced mutations (Supplementary Table S1, (Dvorak et al., 2018)). Replacing His59 with the hydrophobic Phe contributed to the formation of new hydrophobic interactions with the side chains of the following amino acids: Pro65, Pro78, and Cys98 (Fig. 4B). The H59F mutation increased the protein stability by 3 °C (Supplementary Table S1, (Dvorak et al., 2018)). A newly formed hydrogen bond – consequence of the V52T substitution – between the oxygen atom of the hydroxyl group of the side chain of Thr52 and the backbone nitrogen of the Asp54 further contributed to the protein stability (the stabilization effect of this substitution was 2 °C). L92Y substitution led to the formation of new polar contact between the side chains of Tyr92 and Glu100 (ΔT_m 1 °C). The T121P substitution very likely restricts the local conformational flexibility of the loop carrying the mutation which led to protein stabilization by 3 °C (Supplementary Table S1, (Dvorak et al., 2018)). The other two mutations, C96N and S109E, located on the protein surface probably led to enhanced interactions with the surrounding water molecules (the stabilization effect of these substitutions was 2 °C and 1 °C, respectively). The analysis of the FGF2-STAB structure did not provide any explanation for the stabilizing effect of E54D and S94I substitutions (ΔT_m 2 °C and 1 °C, respectively) since no obvious changes in the surrounding microenvironment of the substitutions were identified.

While lowering protein flexibility is often correlated with enhanced thermal stability, it is not always the case. The flexibility of specific protein regions may sometimes allow for better adaptation to environmental changes, such as the binding of ligands, ions, or water molecules. This could result in local conformational adjustments that stabilize the protein at higher temperatures. In the present study, MD analysis revealed that the newly introduced Glu in position 109 is the most flexible residue in FGF2-STAB structure, although the S109E substitution contributes to the protein stability by 1 °C as previously determined by differential scanning calorimetry (Dvorak et al., 2018). The S109E substitution was predicted by evolution-based approach (Dvorak et al., 2018) which identifies conserved residues in multiple sequence alignment of related sequences that are not present in the target protein (Bednar et al., 2015). In our previous work aimed at understanding the molecular basis of the evolution-based mutation in the haloalkane dehalogenase enzyme, we found out that the stabilization of the mutations identified by the evolution-based approach is driven by both entropy and enthalpy contribution, contrary to primarily enthalpy-driven energy-based mutations (Beerens et al., 2018). Stabilization of evolution-based mutations thus can be explained by differences in the solvation, flexibility, and energy of the unfolded state upon introduced mutation. This correlates with our finding that S109E mutation likely enhanced interactions with the surrounding waters and simultaneously increased flexibility of the surface loop (residues 105–112) in which it is located. Except S109E and V52T, the other stabilizing substitutions present in FGF2-STAB were predicted by an energy-based approach (Supplementary Table S1, (Dvorak et al., 2018)) which is primarily enthalpically driven. The enthalpy contribution to protein stability can be interpreted in terms of favorable and unfavorable interactions, such as hydrogen bonds, electrostatics, hydrophobic interactions, and steric clashes, often directly observed in crystal structures. This explains why the most stabilizing substitutions R31L and H59F (ΔT_m 4 and 3 °C, respectively) significantly enhancing intramolecular hydrophobic interactions in FGF2-STAB did not affect the B-factors in MD simulations, since differences in protein flexibility are entropy-driven modifications.

Conclusions

To obtain structural insight into the unique properties of the thermostable nine-point variant of human FGF2, FGF2-STAB, we performed X-ray structural analysis of the protein combined with MD simulations. The crystal structure of FGF2-STAB solved at 1.3 Å resolution revealed high structural similarity of FGF2-STAB with FGF2-wt. A significant difference in flexibility between the surface region of FGF2-STAB and FGF2-wt formed by amino residues 105–112 was identified by analysis

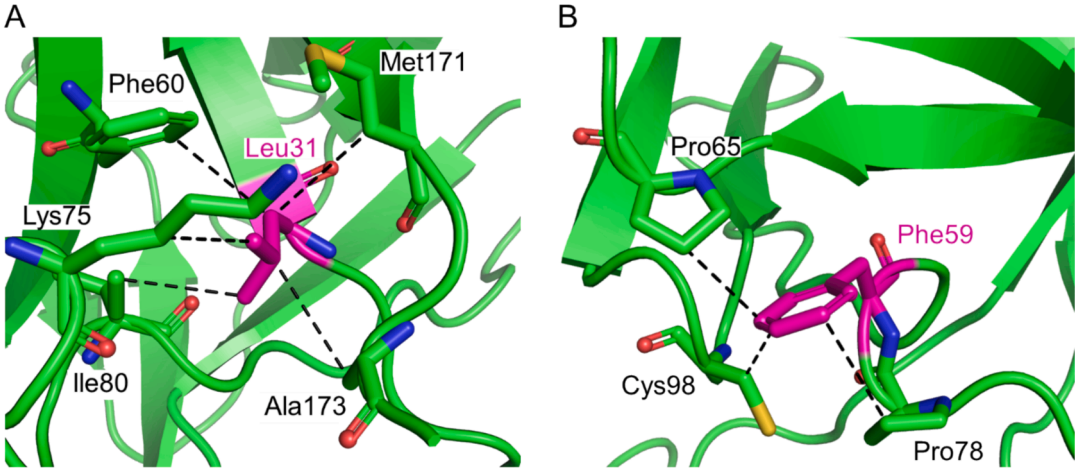

Fig. 4. New hydrophobic interactions (shown by the black dashed lines) formed after the introduction of (A) R31L and (B) H59F substitution into the structure of FGF2-STAB. Interacting amino acids are shown as sticks. The introduced mutations are highlighted in magenta. (For interpretation of the references to color in this figure legend, the reader is referred to the web version of this article.)

of B-factors and evolution of secondary elements during the MD simulations. Increased flexibility of the surface region participating in the binding interaction with the FGF receptor, likely caused by S109E substitution, is probably linked with previously reported enhanced efficiency of FGF2-STAB to induce cell growth response. No structural explanation for the lower dependence of FGF2-STAB on heparin was identified. The enhanced melting temperature of FGF2-STAB can be explained by newly formed hydrophobic interactions introduced by substitutions R31L and H59F, a new hydrogen bond introduced by the V52T substitution, and an additional polar contact introduced by the L92Y substitution. The surface residue substitutions C96N and S109E led to improved interactions with the surrounding water molecules. Our mechanistic study paved the way to engineering other growth factors with enhanced thermostability and preserved biological function.

Declaration of competing interest

Jiri Damborsky, Veronika Stepankova, and Radka Chaloupkova are shareholders of Enantis Ltd, which is the first biotechnology spin-off company of Masaryk University. Gabin de La Bourdonnaye, and Tereza Ghazalova are employees of Enantis Ltd. The authors Martin Marek, Petr Pachl, and Jiri Brynda have no conflicts of interest with the contents of this article. The thermostable variant of FGF2, FGF2-STAB, has been registered with a patent application filed under PCT (WO2017089016A1) and is covered by patent nos. EP3380508B1, US11746135B2, CA3006388C, and JP7131772B2.

CRediT authorship contribution statement

Gabin de La Bourdonnaye: Writing – review & editing, Writing – original draft, Investigation, Formal analysis. **Martin Marek:** Writing – review & editing, Funding acquisition, Formal analysis. **Tereza Ghazalova:** Visualization, Investigation. **Jiri Damborsky:** Investigation, Formal analysis. **Petr Pachl:** Writing – review & editing, Investigation, Formal analysis. **Jiri Brynda:** Investigation, Formal analysis. **Veronika Stepankova:** Funding acquisition, Conceptualization. **Radka Chaloupkova:** Writing – review & editing, Writing – original draft, Visualization, Supervision, Formal analysis, Conceptualization.

Declaration of competing interest

The authors declare the following financial interests/personal relationships which may be considered as potential competing interests: [Veronika Stepankova reports financial support was provided by Enantis. Jiri Damborsky reports a relationship with Enantis that includes: equity or stocks. Veronika Stepankova reports a relationship with Enantis that includes: equity or stocks. Radka Chaloupkova reports a relationship with Enantis that includes: equity or stocks. Gabin de La Bourdonnaye reports a relationship with Enantis that includes: employment. Tereza Ghazalova reports a relationship with Enantis that includes: employment. Radka Chaloupkova, Veronika Stepankova, Jiri Damborsky has patent #Thermostable fgf2 polypeptide, use thereof, WO2017089016A1 issued to Masaryk University and Enantis. If there are other authors, they declare that they have no known competing financial interests or personal relationships that could have appeared to influence the work reported in this paper].

Acknowledgements

The authors would like to acknowledge Assoc. Prof. Pavlina Maloy Rezacova (IOCB CAS, Prague, Czech Republic) for allowing us to test the diffraction quality of the crystals in her laboratory, and to Dr. David Bednar (Masaryk University, Brno, Czech Republic) for the helpful discussion of MD simulation results. Diffraction data have been collected on BL14.1 at the BESSY II electron storage ring operated by the Helmholtz-Zentrum Berlin. This study was supported by the European Union's Horizon 2020 research and innovation programme: the EU ITN ES-Cat (722610), the Technological Agency of the Czech Republic (TH02010219), and the Czech Science Foundation (GA22-09853S). The infrastructures supported by the Ministry of Education, Youth and Sports of the Czech Republic (RECETOX RI LM2023069 and ELIXIR LM2023055) provided the computational resources.

Appendix A. Supplementary data

Supplementary data to this article can be found online at https://doi.org/10.1016/j.yjsbx.2024.100112.

Data availability

Data will be made available on request.

References

Adams, P.D., Afonine, P.V., Bunkóczi, G., Chen, V.B., Davis, I.W., Echols, N., Headd, J.J., Hung, L.-W., Kapral, G.J., Grosse-Kunstleve, R.W., McCoy, A.J., Moriarty, N.W., Oeffner, R., Read, R.J., Richardson, D.C., Richardson, J.S., Terwilliger, T.C., Zwart, P.H., 2010. PHENIX: a comprehensive Python-based system for macromolecular structure solution. Acta Crystallogr D Biol Crystallogr 66, 213–221. https://doi.org/10.1107/S0907444909052925.

Amit, M., Carpenter, M.K., Inokuma, M.S., Chiu, C.-P., Harris, C.P., Waknitz, M.A., Itskovitz-Eldor, J., Thomson, J.A., 2000. Clonally derived human embryonic stem cell lines maintain pluripotency and proliferative potential for prolonged periods of culture. Dev. Biol. 227, 271–278. https://doi.org/10.1006/dbio.2000.9912.

Anandakrishnan, R., Aguilar, B., Onufriev, A.V., 2012. H++ 3.0: automating pK prediction and the preparation of biomolecular structures for atomistic molecular modeling and simulations. Nucleic Acids Res 40, W537–W541. https://doi.org/10.1093/nar/gks375.

Barrientos, S., Brem, H., Stojadinovic, O., Tomic-Canic, M., 2014. Clinical application of growth factors and cytokines in wound healing. Wound Repair Regen 22, 569–578. https://doi.org/10.1111/wrr.12205.

Bednar, D., Beerens, K., Sebestova, E., Bendl, J., Khare, S., Chaloupkova, R., Prokop, Z., Brezovsky, J., Baker, D., Damborsky, J., 2015. FireProt: energy- and evolution-based computational design of thermostable multiple-point mutants. PLoS Comput. Biol. 11, e1004556. https://doi.org/10.1371/journal.pcbi.1004556.

Beerens, K., Mazurenko, S., Kunka, A., Marques, S.M., Hansen, N., Musil, M., Chaloupkova, R., Waterman, J., Brezovsky, J., Bednar, D., Prokop, Z., Damborsky, J., 2018. Evolutionary analysis as a powerful complement to energy calculations for protein stabilization. ACS Catal. 8, 9420–9428. https://doi.org/10.1021/acscatal.8b01677.

Belov, A.A., Mohammadi, M., 2013. Molecular mechanisms of fibroblast growth factor signaling in physiology and pathology. Cold Spring Harb Perspect Biol 5, a015958. https://doi.org/10.1101/cshperspect.a015958.

Bikfalvi, A., Klein, S., Pintucci, G., Rifkin, D.B., 1997. Biological roles of fibroblast growth factor-2. Endocr. Rev. 18, 26–45. https://doi.org/10.1210/edrv.18.1.0292.

Buchtova, M., Chaloupkova, R., Zakrzewska, M., Vesela, I., Cela, P., Barathova, J., Gudernova, I., Zajickova, R., Trantirek, L., Martin, J., Kostas, M., Otlewski, J., Damborsky, J., Kozubik, A., Wiedlocha, A., Krejci, P., 2015. Instability restricts signaling of multiple fibroblast growth factors. Cell Mol Life Sci 72, 2445–2459. https://doi.org/10.1007/s00018-015-1856-8.

Caldararu, O., Kumar, R., Oksanen, E., Logan, D.T., Ryde, U., 2019. Are crystallographic B-factors suitable for calculating protein conformational entropy? Phys Chem Chem Phys 21, 18149–18160. https://doi.org/10.1039/c9cp02504a.

Caldwell, M.A., Garcion, E., terBorg, M.G., He, X., Svendsen, C.N., 2004. Heparin stabilizes FGF-2 and modulates striatal precursor cell behavior in response to EGF. Exp Neurol 188, 408–420. https://doi.org/10.1016/j.expneurol.2004.05.007.

Case, D.A., Aktulga, H.M., Belfon, K., Cerutti, D.S., Cisneros, G.A., Cruzeiro, V.W.D., Forouzesh, N., Giese, T.J., Götz, A.W., Gohlke, H., Izadi, S., Kasavajhala, K., Kaymak, M.C., King, E., Kurtzman, T., Lee, T.-S., Li, P., Liu, J., Luchko, T., Luo, R., Manathunga, M., Machado, M.R., Nguyen, H.M., O'Hearn, K.A., Onufriev, A.V., Pan, F., Pantano, S., Qi, R., Rahnamoun, A., Risheh, A., Schott-Verdugo, S., Shajan, A., Swails, J., Wang, J., Wei, H., Wu, X., Wu, Y., Zhang, S., Zhao, S., Zhu, Q., Cheatham, T.E.I., Roe, D.R., Roitberg, A., Simmerling, C., York, D.M., Nagan, M.C., Merz Jr., K.M., 2023. Ambertools. J Chem Inf Model 63, 6183–6191. https://doi.org/10.1021/acs.jcim.3c01153.

Cerutti, D.S., Swope, W.C., Rice, J.E., Case, D.A., 2014. ff14ipq: A self-consistent force field for condensed-phase simulations of proteins. J Chem Theory Comput 10, 4515–4534. https://doi.org/10.1021/ct500643c.

Chen, V.B., Arendall, W.B., Headd, J.J., Keedy, D.A., Immormino, R.M., Kapral, G.J., Murray, L.W., Richardson, J.S., Richardson, D.C., 2010. MolProbity: all-atom structure validation for macromolecular crystallography. Acta Crystallogr D Biol Crystallogr 66, 12–21. https://doi.org/10.1107/S0907444909042073.

Chen, G., Gulbranson, D.R., Yu, P., Hou, Z., Thomson, J.A., 2012. Thermal stability of fibroblast growth factor protein is a determinant factor in regulating self-renewal, differentiation, and reprogramming in human pluripotent stem cells. Stem Cells 30, 623–630. https://doi.org/10.1002/stem.1021.

Delehedde, M., Lyon, M., Gallagher, J., Rudland, P.S., Fernig, D.G., 2002. Fibroblast growth factor-2 binds to small heparin-derived oligosaccharides and stimulates a sustained phosphorylation of p42/44 mitogen-activated protein kinase and

proliferation of rat mammary fibroblasts. Biochem J 366, 235–244. https://doi.org/10.1042/bj20011718.
Dvorak, P., Bednar, D., Vanacek, P., Balek, L., Eiselleova, L., Stepankova, V., Sebestova, E., Kunova Bosakova, M., Konecna, Z., Mazurenko, S., Kunka, A., Vanova, T., Zoufalova, K., Chaloupkova, R., Brezovsky, J., Krejci, P., Prokop, Z., Dvorak, P., Damborsky, J., 2018. Computer-assisted engineering of hyperstable fibroblast growth factor 2. Biotechnol Bioeng 115, 850–862. https://doi.org/10.1002/bit.26531.
Dvorak, Petr, Krejci, P., Balek, L., Eiselleova, L., Konecna, Z., Dvorak, Pavel, Bednar, D., Brezovsky, J., Sebestova, E., Chaloupkova, R., Stepankova, V., Vanacek, P., Prokop, Z., Damborsky, J., Bosakova, M, M., 2017. Thermostable fgf2 polypeptide, use thereof. WO2017089016A1.
Elber, R., Ruymgaart, A.P., Hess, B., 2011. SHAKE parallelization. Eur Phys J Spec Top 200, 211–223. https://doi.org/10.1140/epjst/e2011-01525-9.
Emsley, P., Lohkamp, B., Scott, W.G., Cowtan, K., 2010. Features and development of Coot. Acta Crystallogr D Biol Crystallogr 66, 486–501. https://doi.org/10.1107/S0907444910007493.
Eriksson, A.E., Cousens, L.S., Matthews, B.W., 1993. Refinement of the structure of human basic fibroblast growth factor at 1.6 A resolution and analysis of presumed heparin binding sites by selenate substitution. Protein Sci 2, 1274–1284. https://doi.org/10.1002/pro.5560020810.
Fannon, M., Nugent, M.A., 1996. Basic fibroblast growth factor binds its receptors, is internalized, and stimulates DNA synthesis in Balb/c3T3 cells in the absence of heparan sulfate. J Biol Chem 271, 17949–17956. https://doi.org/10.1074/jbc.271.30.17949.
Götz, A.W., Williamson, M.J., Xu, D., Poole, D., Le Grand, S., Walker, R.C., 2012. Routine microsecond molecular dynamics simulations with AMBER on GPUs. 1. Generalized Born. J. Chem. Theory Comput. 8, 1542–1555. https://doi.org/10.1021/ct200909j.
Harvey, M.J., De Fabritiis, G., 2009. An implementation of the smooth particle mesh ewald method on GPU hardware. J Chem Theory Comput 5, 2371–2377. https://doi.org/10.1021/ct900275y.
Hui, Q., Jin, Z., Li, X., Liu, C., Wang, X., 2018. FGF family: from drug development to clinical application. Int J Mol Sci 19, 1875. https://doi.org/10.3390/ijms19071875.
Ibrahimi, O.A., Zhang, F., Lang Hrstka, S.C., Mohammadi, M., Linhardt, R.J., 2004. Kinetic model for FGF, FGFR, and proteoglycan signal transduction complex assembly. Biochemistry 43, 4724–4730. https://doi.org/10.1021/bi0352320.
Javerzat, S., Auguste, P., Bikfalvi, A., 2002. The role of fibroblast growth factors in vascular development. Trends Mol Med 8, 483–489. https://doi.org/10.1016/s1471-4914(02)02394-8.
Karplus, P.A., Diederichs, K., 2012. Linking crystallographic model and data quality. Science 336, 1030–1033. https://doi.org/10.1126/science.1218231.
Koledova, Z., Sumbal, J., Rabata, A., Bourdonnaye, G.de.L., Chaloupkova, R., Hrdlickova, B., Damborsky, J., Stepankova, V., 2019. Fibroblast growth factor 2 protein stability provides decreased dependence on heparin for induction of FGFR signaling and alters ERK signaling dynamics. Front Cell Dev Biol 7, 331. https://doi.org/10.3389/fcell.2019.00331.
La Venuta, G., Zeitler, M., Steringer, J.P., Müller, H.-M., Nickel, W., 2015. The startling properties of fibroblast growth factor 2: how to exit mammalian cells without a signal peptide at hand. J Biol Chem 290, 27015–27020. https://doi.org/10.1074/jbc.R115.689257.
Levenstein, M.E., Ludwig, T.E., Xu, R.-H., Llanas, R.A., VanDenHeuvel-Kramer, K., Manning, D., Thomson, J.A., 2006. Basic fibroblast growth factor support of human embryonic stem cell self-renewal. Stem Cells 24, 568–574. https://doi.org/10.1634/stemcells.2005-0247.
Lotz, S., Goderie, S., Tokas, N., Hirsch, S.E., Ahmad, F., Corneo, B., Le, S., Banerjee, A., Kane, R.S., Stern, J.H., Temple, S., Fasano, C.A., 2013. Sustained levels of FGF2 maintain undifferentiated stem cell cultures with biweekly feeding. PLoS One 8, e56289. https://doi.org/10.1371/journal.pone.0056289.
Mueller, U., Förster, R., Hellmig, M., Huschmann, F.U., Kastner, A., Malecki, P., Pühringer, S., Röwer, M., Sparta, K., Steffien, M., Ühlein, M., Wilk, P., Weiss, M.S., 2015. The macromolecular crystallography beamlines at BESSY II of the Helmholtz-Zentrum Berlin: Current status and perspectives. Eur Phys J Plus 130, 141–150. https://doi.org/10.1140/epjp/i2015-15141-2.
Murshudov, G.N., Skubák, P., Lebedev, A.A., Pannu, N.S., Steiner, R.A., Nicholls, R.A., Winn, M.D., Long, F., Vagin, A.A., 2011. REFMAC5 for the refinement of macromolecular crystal structures. Acta Crystallogr D Biol Crystallogr 67, 355–367. https://doi.org/10.1107/S0907444911001314.
Murzin, A.G., Lesk, A.M., Chothia, C., 1992. beta-Trefoil fold. Patterns of structure and sequence in the Kunitz inhibitors interleukins-1 beta and 1 alpha and fibroblast growth factors. J Mol Biol 223, 531–543. https://doi.org/10.1016/0022-2836(92)90668-a.
Nugent, M.A., Edelman, E.R., 1992. Kinetics of basic fibroblast growth factor binding to its receptor and heparan sulfate proteoglycan: a mechanism for cooperactivity. Biochemistry 31, 8876–8883. https://doi.org/10.1021/bi00152a026.
Nugent, M.A., Iozzo, R.V., 2000. Fibroblast growth factor-2. Int J Biochem Cell Biol 32, 115–120. https://doi.org/10.1016/S1357-2725(99)00123-5.
Ornitz, D.M., Itoh, N., 2015. The fibroblast growth factor signaling pathway. Wiley Interdiscip Rev Dev Biol 4, 215–266. https://doi.org/10.1002/wdev.176.
Paluck, S.J., Nguyen, T.H., Lee, J.P., Maynard, H.D., 2016. A Heparin-mimicking block copolymer both stabilizes and increases the activity of fibroblast growth factor 2 (FGF2). Biomacromolecules 17, 3386–3395. https://doi.org/10.1021/acs.biomac.6b01182.
Plotnikov, A.N., Schlessinger, J., Hubbard, S.R., Mohammadi, M., 1999. Structural basis for FGF receptor dimerization and activation. Cell 98, 641–650. https://doi.org/10.1016/s0092-8674(00)80051-3.
Plotnikov, A.N., Hubbard, S.R., Schlessinger, J., Mohammadi, M., 2000. Crystal structures of two FGF-FGFR complexes reveal the determinants of ligand-receptor specificity. Cell 101, 413–424. https://doi.org/10.1016/s0092-8674(00)80851-x.
Salomon-Ferrer, R., Götz, A.W., Poole, D., Le Grand, S., Walker, R.C., 2013. Routine microsecond molecular dynamics simulations with AMBER on GPUs. 2. explicit solvent particle mesh ewald. J Chem Theory Comput 9, 3878–3888. https://doi.org/10.1021/ct400314y.
Vagin, A., Teplyakov, A., 2010. Molecular replacement with MOLREP. Acta Crystallogr D Biol Crystallogr 66, 22–25. https://doi.org/10.1107/S0907444909042589.
Winn, M.D., Ballard, C.C., Cowtan, K.D., Dodson, E.J., Emsley, P., Evans, P.R., Keegan, R.M., Krissinel, E.B., Leslie, A.G.W., McCoy, A., McNicholas, S.J., Murshudov, G.N., Pannu, N.S., Potterton, E.A., Powell, H.R., Read, R.J., Vagin, A., Wilson, K.S., 2011. Overview of the CCP4 suite and current developments. Acta Crystallogr D Biol Crystallogr 67, 235–242. https://doi.org/10.1107/S0907444910045749.
Xu, C., Rosler, E., Jiang, J., Lebkowski, J.S., Gold, J.D., O'Sullivan, C., Delavan-Boorsma, K., Mok, M., Bronstein, A., Carpenter, M.K., 2005. Basic fibroblast growth factor supports undifferentiated human embryonic stem cell growth without conditioned medium. Stem Cells 23, 315–323. https://doi.org/10.1634/stemcells.2004-0211.
Yun, Y.-R., Won, J.E., Jeon, E., Lee, S., Kang, W., Jo, H., Jang, J.-H., Shin, U.S., Kim, H.-W., 2010. Fibroblast growth factors: biology, function, and application for tissue regeneration. J Tissue Eng 2010, 218142. https://doi.org/10.4061/2010/218142.
Zakrzewska, M., Krowarsch, D., Wiedlocha, A., Olsnes, S., Otlewski, J., 2005. Highly stable mutants of human fibroblast growth factor-1 exhibit prolonged biological action. J Mol Biol 352, 860–875. https://doi.org/10.1016/j.jmb.2005.07.066.
Zehe, C., Engling, A., Wegehingel, S., Schäfer, T., Nickel, W., 2006. Cell-surface heparan sulfate proteoglycans are essential components of the unconventional export machinery of FGF-2. Proc Natl Acad Sci U S A 103, 15479–15484. https://doi.org/10.1073/pnas.0605997103.
Zhang, J.D., Cousens, L.S., Barr, P.J., Sprang, S.R., 1991. Three-dimensional structure of human basic fibroblast growth factor, a structural homolog of interleukin 1 beta. Proc Natl Acad Sci U S A 88, 3446–3450. https://doi.org/10.1073/pnas.88.8.3446.
Zhu, H., Duchesne, L., Rudland, P.S., Fernig, D.G., 2010. The heparan sulfate co-receptor and the concentration of fibroblast growth factor-2 independently elicit different signalling patterns from the fibroblast growth factor receptor. Cell Commun Signal 8, 14. https://doi.org/10.1186/1478-811X-8-14.